Article

Short-term in vivo biological and mechanical remodeling of porcine acellular dermal matrices

Journal of Tissue Engineering
4: 2041731413490182

DOI: 10.1177/2041731413490182
tej.sagepub.com
SAGE

Gary A. Monteiro, Neil L. Rodriguez, Aubrey I. Delossantos and Christopher T. Wagner

Abstract

The purpose of this study was to assess the biological revitalization and mechanical integrity of Strattice™ Reconstructive Tissue Matrix, a porcine-derived acellular dermal matrix, in vivo over time. We expanded the traditional subcutaneous model to incorporate biologic matrix scaffolds large enough to allow evaluation of mechanical properties in addition to the assessment of histological changes. Hematoxylin and eosin histology staining was used to evaluate cellular and tissue changes, and a mechanical testing frame was used to measure the ultimate tensile stress and Young's modulus of the implanted material over time. Cell infiltration and blood vessel formation into the porcine-derived acellular dermal matrix were evident at 2 weeks and increased with implantation time. Mechanical remodeling resulted in an initial decrease in ultimate tensile stress, not associated with cell infiltration, followed by a significant increase in material strength, concurrent with histological evidence of new collagen synthesis. Young's modulus followed a similar trend.

Keywords

Strattice, extracellular matrix, tissue matrix, regeneration

Introduction

Biological scaffolds derived from xenogeneic sources are increasingly used clinically during abdominal wall repair[1–3] and breast reconstruction procedures.[4] In general, surgeons have different preferences with respect to the handling of biological matrices: stiff materials that do not stretch or elongate under constant load are preferred to repair abdominal wall defects. Depending on surgical technique, such materials provide scaffolds that may resist bulging and defect recurrence. More compliant materials that conform to the natural contours of the body are typically preferred for breast reconstruction. Several biologically derived matrix materials are commercially available for surgical use.[5–8] To differentiate these products, manufacturers often compare out-of-package material properties.[6,8–10] However, while it is important to understand these properties for handling considerations, it is imperative to recognize that most biological materials, depending on the production processing, will change once implanted and remodel over time.[11–16] Therefore, it is more important to understand postimplantation behavior as compared to ex vivo performance requirements for matrices that are expected to be incorporated into the natural anabolic and catabolic processes of the recipient. The biological revitalization (recellularization and blood vessel formation) and inflammatory response of the product used for repair or reconstruction will affect the integrity and mechanical properties of the repair over time[12,13,16] and, ultimately, the long-term success of the surgical procedure.

Strattice™ Reconstructive Tissue Matrix (LifeCell Corporation, Branchburg, NJ, USA) is a commercially available biological matrix scaffold used for tissue repair and reconstruction. It is derived from porcine dermis and undergoes a minimally manipulative proprietary process that removes cells in order to minimize an antigenic response as well as significantly reduce the key component (1,3 alpha-galactose moiety) attributed to play a major role in the acute xenogeneic rejection response. The processing is used to prepare intact extracellular matrix (ECM)-based scaffolds with distinct handling characteristics. Strattice matrices can be broadly classified into two types: pliable

LifeCell Corporation, Branchburg, NJ, USA

Corresponding author:
Gary A Monteiro, LifeCell Corporation, One Millennium Way, Branchburg, NJ 08876, USA.
Email: gmonteiro@lifecell.com

and firm. Each has unique physical properties that provide options to the surgeon to use a matrix suited to support different soft-tissue repair applications and procedures. Previous work has demonstrated the capability of ECM-based scaffolds to remodel over time; explants from a primate abdominal wall defect model demonstrated that revascularization and repopulation in ECM-based scaffolds occurred by 2 weeks and collagen reorganization by 180 days.[17,18] While it is clear from these studies that the integration and strength of the Strattice matrix exceed the functional requirements in the model evaluated, the early kinetics of mechanical and biological remodeling are not completely understood. Both ethics and cost make evaluating the short-term kinetics of biological scaffold remodeling in a primate model impractical.

One approach to better understand the in vivo remodeling kinetics of biological ECM-based scaffolds is to evaluate the biological response of the material in a rat subcutaneous model. Such models have routinely been used to evaluate the biological performance and compatibility of materials used for clinical implantation.[19–22] Typically, a 1 × 1-cm piece of material is implanted in the connective tissue of a subcutaneous pocket, explanted at predetermined time points, and evaluated using standard histological and scoring methods. Parameters that are generally evaluated include cell infiltration, blood vessel formation, and inflammatory cell responses. Although this approach is extremely valuable in determining a material's biological response and safety, it does not provide direct evidence of the mechanical remodeling of the biological scaffold. Furthermore, mechanical testing of such small implants is inordinately affected by the short gauge length of the sample. Understanding the mechanical remodeling of biological scaffolds is pertinent for load-bearing or wound-reinforcing scaffolds. Herein, we have extended a rat subcutaneous pocket model to allow implantation of a tissue sample large enough for concurrent evaluation of both biological and mechanical properties. The purpose of this study was to evaluate the short-term in vivo kinetics of mechanical and biological remodeling of intact acellular ECM scaffolds. We hypothesized that there would be detectable temporal differences in the mechano-physical integrity as a result of the biological response of the implanted matrix material.

Methods and materials

Porcine dermis processing

Porcine-derived acellular dermal matrix (PADM; Strattice) was prepared as per the study by Connor et al.[18] Following preparation, PADM samples were terminally sterilized. Time-zero control testing resulted in biological and mechanical characteristics as previously described.[18] PADM samples were prepared as 2 × 6-cm pieces and grouped into pliable and firm handling characteristics of the commercial product. The target split thickness, prior to processing, for firm material was set at 1.3 mm and for pliable material was set at 1.0 mm.

In vivo study design and animal model

The study protocol was approved by the appropriate Institutional Animal Care and Use Committee (IACUC) prior to commencing the study, which was conducted at an Association for Assessment and Accreditation of Laboratory Animal Care International—accredited facility registered with the United States Department of Agriculture (Northwood, OH).

In this study, 36 immune-competent male Lewis rats, each weighing between 300 and 350 g, were used, and PADM firm and PADM pliable materials were implanted. A randomization scheme was used to implant the materials on the left or right side of the animal. Six replicates per study arm ($n = 6$) were implanted for each time point. All materials were handled aseptically. Prior to implantation, each 2 × 6-cm sample was measured to ensure that all implants were within a tolerance of ±0.2 cm in length and width. Samples were trimmed if necessary. Immediately prior to implantation, each test sample was rinsed in fresh sterile saline solution for 2–4 min.

An incision was made on the right caudal and cranial end of the skin and perpendicular to the thoracic–lumbar region of the vertebral column. A pocket was tunneled by blunt dissection in the subcutaneous tissue between the two incisions. One article was implanted in the pocket. Care was taken to ensure that the article was lying flat in the pocket. A second test article was implanted in the contralateral side using the same technique. The skin was closed at the tunnel ends with appropriate stainless steel wound clips. A schematic of the implantation design is presented in Figure 1. Following implantation, the animals were observed daily to ensure IACUC recovery and outcomes. Animals were euthanized, and explants were harvested every 5 days until day 30 postimplantation.

Explant gross observations

Gross observations were noted at the time of material explant. These included hematomas, breach of abdominal cavity, adhesions, folding of tissue, or explant overlap. The 2 × 6-cm explant was cut into half longitudinally to produce one 1 × 6-cm sample for mechanical testing and one paired 1 × 6-cm sample for histological analysis (Figure 1).

Tensile testing

Tensile testing was performed on 1 × 6-cm strips of PADM fully hydrated in 0.9% saline. Prior to tensile testing, surrounding connective tissue was excised, and sample

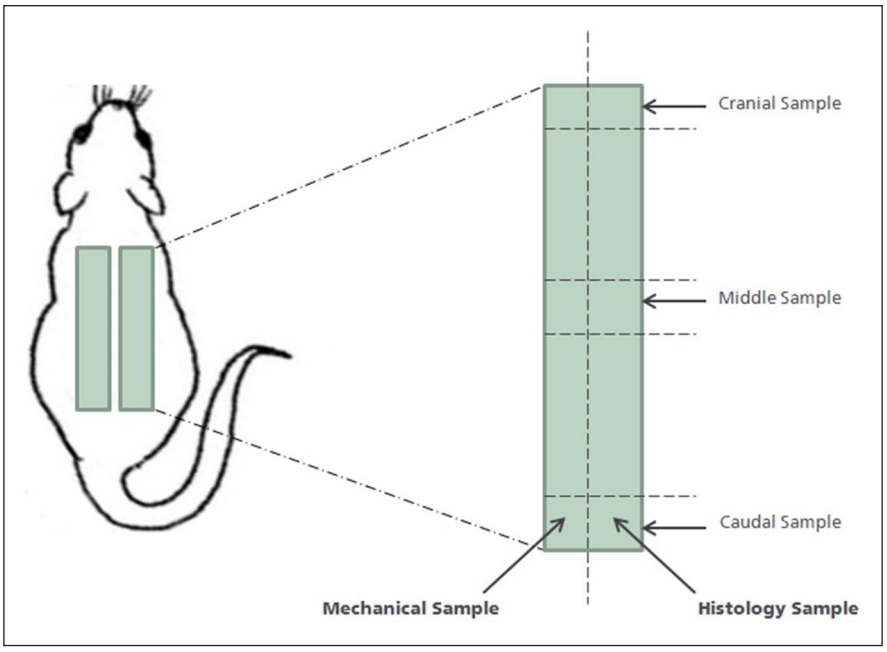

Figure 1. Explant sampling scheme. Two 2 × 6-cm pieces of PADM from each process were implanted in a subcutaneous pocket on the back of a rat. A total of 36 PADM samples were implanted for each process method. Six PADM samples were harvested at each time point, once a week for 6 weeks. One half of the explanted PADM sample was used for mechanical evaluation and the other half was used for histological evaluation.
PADM: porcine-derived acellular dermal matrix.

thicknesses were measured using a Mitutoyo Low Force Digital Indicator (Aurora, IL, USA). Sample thicknesses were measured to capture swelling of materials during processing as well as remodeling in vivo. Samples were placed between pneumatic grips attached to a 5865 Electromechanical Tensile Testing frame fitted with a 1.0-kN load cell (Instron Corporation, Norwood, MA, USA) such that the final gripped sample had a 4 cm gauge length. Samples were then preloaded to 0.2 N and pulled at a strain rate of 1.65% per minute (0.66 mm/min) to a failure or a load drop of 60% or greater above a threshold of 6 N while recording load and displacement data. Following testing, stress (force per unit area of cross section), strain at 30 N (change in sample length at 30 N divided by original length), and Young's modulus (slope of linear region in the stress strain curve) were calculated using standard algorithms in Bluehill® 2 software (Instron Corporation). All load extension curves generated were manually reviewed to ensure accuracy of the calculated values.

Explant histology

Three histology samples were biopsied from across each 1 × 6-cm section of explant designated for histology: cranial, middle, and caudal. Biopsies were fixed in 10% neutral buffered formalin and processed and thin-sectioned for either hematoxylin and eosin (H&E) or Masson's trichrome staining. H&E slides were evaluated for cellularity (characterized by the presence of fibroblast-like cells), vascularity, and inflammatory cell infiltration by a blinded subject matter expert using a scoring system of 0–3, with 0–1 being none, 1–2 being minimal, 2–3 being moderate, and 3 being significant. Trichrome slides were evaluated for the presence of new formed collagen. The intensity of the trichrome staining was used as a measure of collagen fiber density and maturation (loose and lighter blue fibers indicate newly formed collagen bundles, and densely organized darker blue staining indicates older, more mature collagen bundles).

Statistical analysis

Minitab® Statistical Software version 16.2.0 (Minitab Inc., State College, PA, USA) was used to perform all statistical analyses. Differences in mechanical properties between conditions were assessed using a general linear model followed by Tukey's post hoc test, with $p < 0.05$ considered significant. Histology results were summarized in chi-square tables.

Confirmatory study

On completion of the above-listed study design, a second study design, to verify results, was executed. The confirmatory study design included only firm PADM with an additional explant time point, beyond that of the original study,

Table 1. Summary of strain at 30 N, ultimate tensile stress, and Young's modulus (average ± standard deviation) of PADM firm and pliable (with and without folds) over time.

Day	Test article	Average ultimate tensile load (N/cm)	Average ultimate tensile stress (MPa)	Strain at 30 N	Average Young's modulus (MPa)
5	Pliable with fold	152 ± 44	12.36 ± 2.31	0.39 ± 0.12	48.26 ± 2.04
10	Pliable with fold	139 ± 44	11.70 ± 2.30	0.40 ± 0.12	53.9 ± 4.31
15	Pliable with fold	119 ± 11	9.37 ± 1.83	0.53 ± 0.09	38.88 ± 16.25
20	Pliable with fold	47 ± 24	4.47 ± 1.88	0.62 ± 0.17	13.73 ± 7.52
25	Pliable with fold	34 ± 9	2.74 ± 0.62	0.54 ± 0.08	9.91 ± 4.68
30	Pliable with fold	No sample with folds			
0	Pliable	206 ± 62	16.01 ± 3.66	0.39 ± 0.07	44.54 ± 10.82
5	Pliable	181 ± 45	14.13 ± 2.31	0.36 ± 0.12	49.11 ± 6.04
10	Pliable	176 ± 34	13.28 ± 2.30	0.32 ± 0.12	58.04 ± 23.38
15	Pliable	124 ± 11	8.77 ± 1.83	0.56 ± 0.09	43.64 ± 21.25
20	Pliable	52 ± 20	4.43 ± 1.88	0.56 ± 0.17	17.55 ± 8.42
25	Pliable	84 ± 18	5.43 ± 0.62	0.54 ± 0.08	21.13 ± 3.43
30	Pliable	108 ± 27	8.87 ± 4.39	0.61 ± 0.25	29.70 ± 21.60
0	Firm	235 ± 32	15.79 ± 1.72	0.17 ± 0.03	65.56 ± 15.82
5	Firm	214 ± 31	16.61 ± 2.09	0.16 ± 0.04	73.94 ± 9.16
10	Firm	174 ± 36	10.65 ± 1.72	0.19 ± 0.03	49.28 ± 13.39
15	Firm	183 ± 68	12.45 ± 2.94	0.22 ± 0.05	55.96 ± 9.08
20	Firm	71 ± 8	5.52 ± 1.03	0.35 ± 0.13	20.92 ± 4.29
25	Firm	52 ± 11	3.53 ± 0.83	0.40 ± 0.10	15.01 ± 3.34
30	Firm	122 ± 27	8.80 ± 1.89	0.30 ± 0.07	38.12 ± 3.76

PADM: porcine-derived acellular dermal matrix.
On average there was an initial decrease up until day 25 of implantation followed by a significant increase between days 25 and 30 in both ultimate tensile stress and Young's modulus. The strain at 30 N increased until day 25 and decreased between days 25 and 30 for all data without folds.

at 42 days. The additional time point was included to confirm trends noted in the original study. All other analyses and methods were similar to that of the original study.

Results

Gross observation

During explantation, the integration of the implant to the surrounding connective tissue was noted. Overall, graft incorporation with native tissue increased over time for both PADM firm and pliable materials. Minimal incorporation was noted at 1 and 2 weeks, and partial incorporation was noted in all samples. Beyond 3 weeks, thickening of connective tissue and vascularity around and into the implants was observed for all samples. The connective tissue around the graft was easily dissected away from the implant using blunt dissection techniques. At no time point was there any evidence of biomaterial-mediated fibrosis at the site of implantation. Minimum to no encapsulation was noted for both PADM material types; these findings were confirmed by histological analysis. Pliable materials were more likely to fold on an edge compared with firm materials. Of the 36 pliable implants, 16 had folds on at least one edge at the time of explanation compared with only 1 of the 36 firm samples. Four hematomas were noted in the PADM firm group and one hematoma was noted in the PADM pliable group.

Tensile material testing

The mechanical properties of explanted materials, freed from surrounding connective tissue, were evaluated on an Instron mechanical tester. Due to the significant number of folds present in the PADM pliable material arm, a retrospective evaluation of the ultimate tensile stress of PADM pliable folded explant material with respect to PADM pliable nonfolded explant material was conducted to determine the influence of folds on mechanical properties of implanted material (Table 1). A general linear model with days and folds was performed to evaluate statistical differences between the maximum stress of materials with and without folds. Statistical differences in the ultimate tensile stress were noted across both days and materials with and without folds (analysis of variance (ANOVA), $p < 0.001$ and $p < 0.001$, respectively). The ultimate tensile stresses of folded samples (8.49 ± 4.57 MPa) were significantly different (lower) than the rest of the sample population (10.43 ± 5.2 MPa) and were therefore removed from subsequent mechanical analysis.

Ultimate tensile stress values and Young's modulus values for both PADM firm and pliable materials were plotted as a function of implantation time (Figure 2). Time-zero values were obtained from samples that were not implanted in the animals. Average values with standard deviation of ultimate tensile stress, strain at 30 N, and Young's modulus are presented in Table 1. In general, ultimate tensile stress

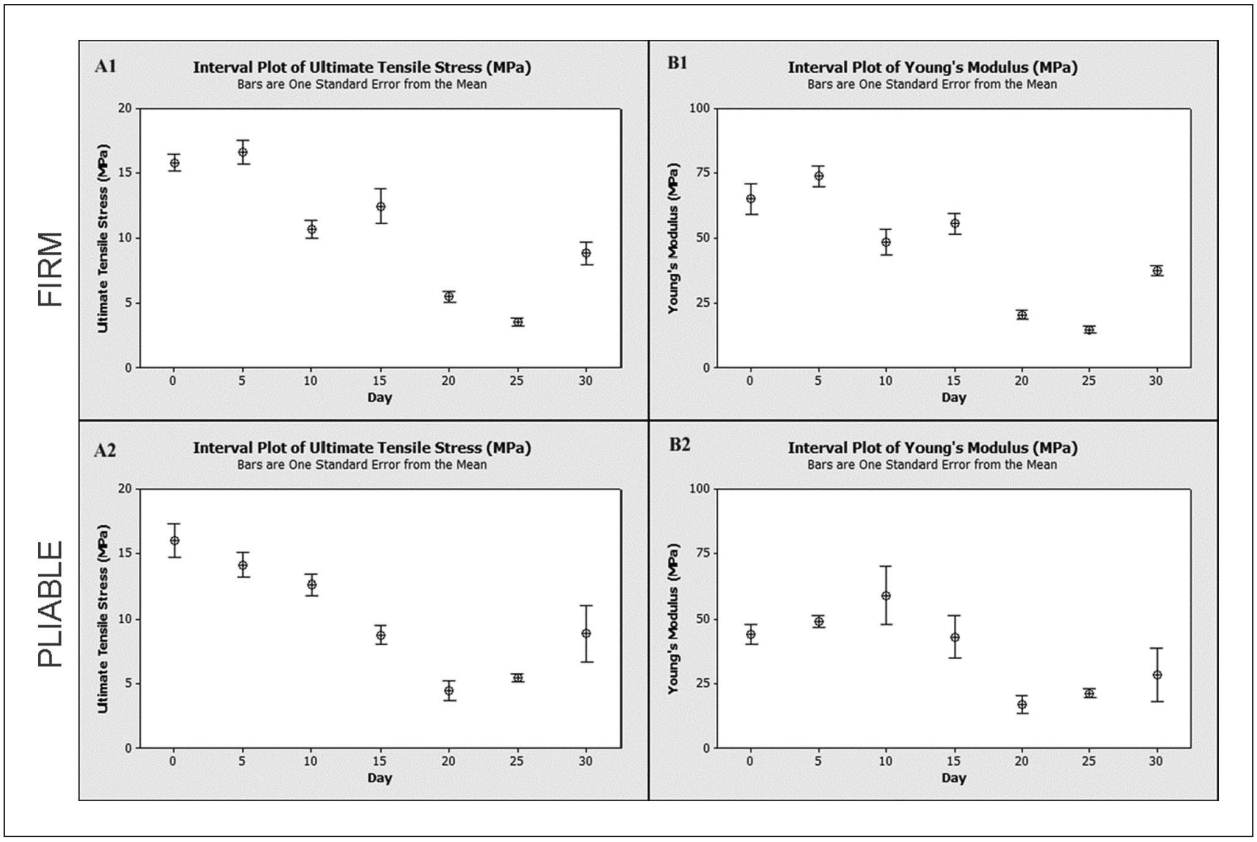

Figure 2. Tensile properties of (1) PADM firm and (2) pliable over time. (A) Ultimate tensile stress and (B) Young's modulus. Tensile properties were measured using an Instron 5680 fitted with a 1-kN load cell and pneumatic grips. On average, there was an initial decrease until day 25 of implantation followed by a significant increase between days 25 and 30 in both ultimate tensile stress and Young's modulus.
PADM: porcine-derived acellular dermal matrix.

and Young's modulus for both PADM firm and pliable material decreased until day 25, followed by a significant increase on day 30. No trend in the thickness measurements was noted (data not shown). (The strain at 30 N increased until day 25, followed by a significant decrease.) A general linear model with day, scaffold type, and the interaction between day and scaffold type was used to determine significance of thickness, ultimate tensile stress, strain at 30 N, and Young's modulus between groups and days.

Significant differences in thickness were noted across days (ANOVA, $p < 0.02$) but not across scaffold types (ANOVA, $p > 0.692$). On average, day 10 samples were 1.6 ± 0.3 mm and day 20 samples were 1.3 ± 0.2 mm. No other statistical differences in thickness were noted across other time points. For the ultimate tensile stress, a significant difference between days was noted (ANOVA, $p < 0.001$). No significant difference in the ultimate tensile stress between scaffold type and the interaction between scaffold type and days was noted (ANOVA, $p > 0.692$ and $p > 0.285$, respectively). A post hoc analysis for comparison between days showed significant differences between days 0 and 5 (Tukey's, $p < 0.0001$ and $p < 0.0020$, respectively) with respect to all other time points. Significant differences were also noted between day 25 and all other time points except day 20 (day 20, Tukey's, $p > 0.754$). No difference in the ultimate tensile stress was noted between day 30 and days 10, 15, and 20 samples (Tukey's, $p > 0.998$, $p > 0.119$, and $p > 0.08$, respectively).

For Young's modulus, significant differences between days as well as specimens were noted (ANOVA, $p < 0.021$ and $p < 0.001$, respectively). No significant difference in Young's modulus was noted in the interaction between material type and days (ANOVA, $p > 0.763$). A post hoc analysis for comparison between days showed significant differences between days 0 and 5 with respect to all time points beyond day 15 (Tukey's, $p < 0.002$ and $p < 0.004$, respectively). Day 15 samples were not significantly different from day 30 time points (Tukey's, $p > 0.883$) but were significantly different from day 20 and day 25 samples (Tukey's, $p < 0.026$ and $p < 0.012$, respectively). No difference in Young's modulus between days 20 and 30 was noted. A confirmatory study to evaluate trends was conducted. Material mechanical properties are summarized in Table 2.

Table 2. Summary of strain at 30 N, ultimate tensile stress, and Young's modulus (average ± standard deviation) of PADM firm over time (confirmatory study).

Day	Average ultimate tensile stress load (N/cm)	Average ultimate tensile stress (MPa)	Strain at 30 N	Average Young's modulus (MPa)
0	255 ± 21	17.6 ± 4.5	0.10 ± 0.02	71.3 ± 6.2
7	346 ±18	22.1 ± 1.1	0.13 ± 0.02	86.7 ± 9.6
14	216 ± 42	14.3 ± 2.5	0.16 ± 0.03	58.6 ± 8.2
21	197 ± 29	13.7 ± 1.7	0.18 ± 0.02	61.0 ± 5.9
28	119 ± 26	7.9 ± 1.7	0.22 ± 0.09	36.4 ± 8.0
35	158 ± 31	10.2 ±1.7	0.16 ± 0.04	50.3 ± 6.6
42	194 ± 25	11.7 ± 1.7	0.14 ± 0.02	53.0 ± 8.1

PADM: porcine-derived acellular dermal matrix.
On average, there was an initial decrease up until day 28 of implantation followed by a significant increase between days 28 and 42 in both ultimate tensile stress and Young's modulus.

Table 3. Explant histology scores tabulated.

	Day	Firm				Pliable			
		None	Minimal	Moderate	Significant	None	Minimal	Moderate	Significant
Inflammatory cell infiltration	5	9	6	3	0	17	1	0	0
	10	0	18	0	0	5	12	0	1
	15	1	15	1	0	0	16	2	0
	20	2	12	3	0	5	12	0	0
	25	1	17	0	1	3	14	0	0
	30	0	16	2	0	2	16	0	0
Revascularization	5	17	1	0	0	18	0	0	0
	10	10	8	0	0	12	6	0	0
	15	3	10	4	0	6	11	1	0
	20	1	9	6	1	2	10	5	0
	25	1	7	8	2	1	9	6	1
	30	1	6	6	5	2	7	8	1
Recellularization	5	13	0	0	0	5	13	0	0
	10	0	18	0	0	0	16	2	0
	15	0	11	6	0	0	14	4	0
	20	0	7	8	2	0	8	8	1
	25	0	4	11	3	0	3	12	2
	30	0	4	8	6	0	3	13	2

PADM: porcine-derived acellular dermal matrix.
At least six slides with three sections—cranial, middle, and caudal (see Figure 1)—at each time point were evaluated for PADM firm and PADM pliable. Each cell represents the number of samples categorized within the specific grouping. Fibroblastic cell infiltration and revascularization of scaffolds increased with time while minimum to mild levels of inflammatory cell infiltration was noted in both PADM firm and pliable.

Histology

H&E scores are summarized in Table 3. Both PADM firm and pliable implants showed an increase in cell infiltration scores for 3 weeks followed by a plateau until day 30. Vascularity also followed a similar trend. Both PADM firm and pliable materials had none to minimal inflammation over the course of the study. Figure 3 shows representative H&E micrographs.

Trichrome-stained slides for both PADM firm and pliable were assessed to measure the new collagen formation. Representative images for PADM firm are shown in Figure 4. For both PADM material types, trichrome staining on day 0 showed dense collagen bundles that progressively loosened through day 25. Increased separation and white space between and across collagen bundles were noted from days 0 through 20. Collagen trichrome staining between days 20 and 30 suggested a substantial increase in density of collagen bundles. Decreased white space and bundle separation were observed from days 20 to 30. Subtle differences in the intensity of blue staining, which differentiate newer collagen (lighter blue) from older collagen (darker blue), were also noted from days 10 to 30 between existing collagen bundles. A confirmatory study to evaluate trends was conducted. Histological evaluation is summarized in Table 4.

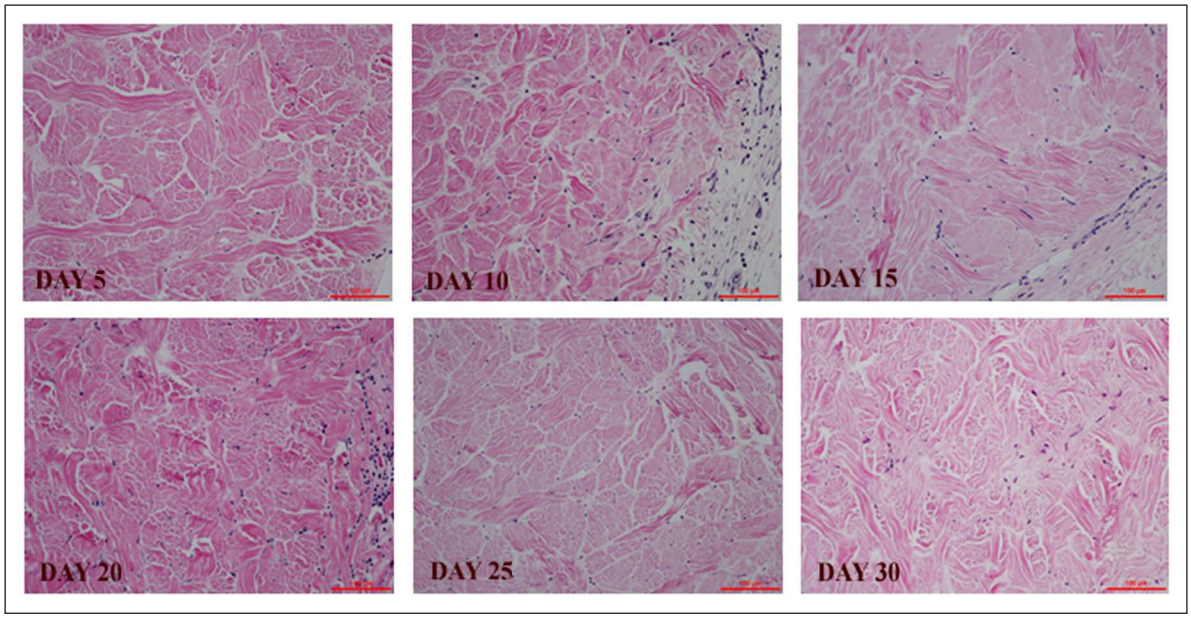

Figure 3. Recellularization and revascularization of implanted PADM materials over time. H&E staining showed cellular content from days 5 to 30. Scale bar is 100 µm. Histology scores are summarized in Table 3.
PADM: porcine-derived acellular dermal matrix; H&E: hematoxylin and eosin.

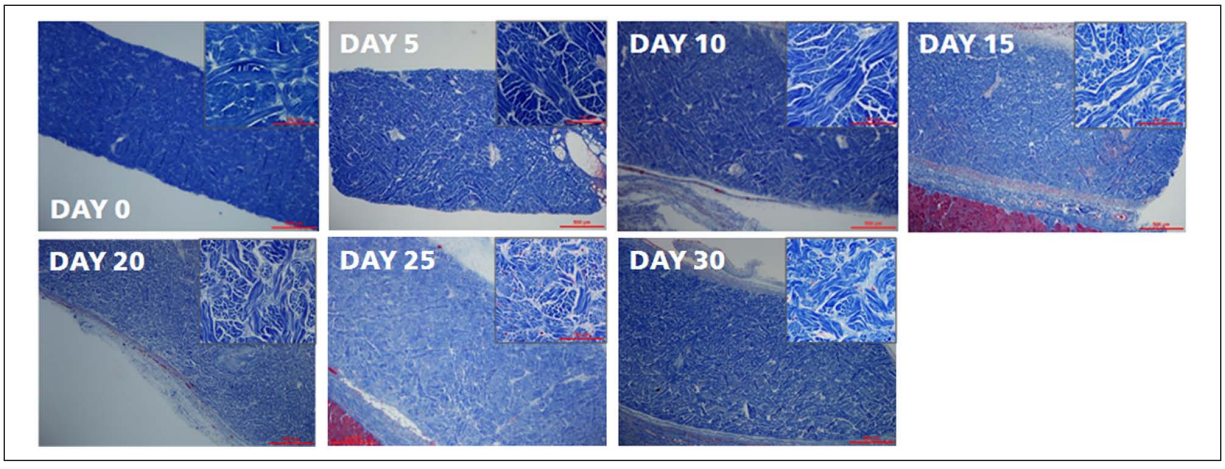

Figure 4. Low- and high-magnification images of PADM firm materials stained with trichrome blue. Trichrome staining on day 0 showed dense collagen bundles that progressively loosened through day 25. Increased separation and white space between and across collagen bundles were noted from days 0 to 20. Collagen staining between days 20 and 30 showed a substantial increase in the density of bundles. Decreased white space and bundle separation were observed from days 20 to 30. Subtle differences in the intensity of blue staining, meant to differentiate newer collagen (lighter blue) from older collagen (darker blue), was also noted from days 10 to 30 between existing collagen bundles. These slides were not scored.
PADM: porcine-derived acellular dermal matrix.

Discussion

This study describes an animal model capable of simultaneously evaluating the short-term in vivo kinetics of biological and mechanical remodeling of intact ECM-based scaffolds. Adding mechanical analysis to the traditional rat subcutaneous model provides valuable information that can act as a surrogate to help understand temporal changes in structural scaffold protein synthesis and remodeling. ECM synthesis and reorganization is necessary for material property changes in intact ECM-based scaffolds. It can be challenging to distinguish native scaffold proteins from newly synthesized proteins using standard histochemical approaches; therefore, the onset of matrix synthesis and biological scaffold remodeling may be missed. Additionally, the presence of newly formed collagen does not always translate to added material strength.[23]

Table 4. Explant histology scores tabulated (confirmatory study).

	Day	Firm			
		None	Minimal	Moderate	Significant
Inflammatory cell infiltration	7	0	5	0	0
	14	0	4	2	0
	21	0	5	1	0
	28	0	6	0	0
	35	0	6	0	0
	42	0	6	0	0
Revascularization	7	5	0	0	0
	14	0	6	0	0
	21	0	5	1	0
	28	0	5	1	0
	35	0	2	4	0
	42	0	3	3	0
Recellularization	7	0	5	0	0
	14	0	6	0	0
	21	0	3	3	0
	28	0	2	4	0
	35	0	1	5	0
	42	0	0	5	1

Trends in recellularization, revascularization, and inflammatory cell response were similar to that seen in the main study.

Both PADM firm and pliable materials were implanted in the model and their biological and mechanical performances were evaluated over time. Substantial biological and mechanical changes in both materials were noted over the study duration. The kinetics of the ultimate tensile stress remodeling and the extension at 30 N for both PADM firm and pliable material followed similar trends. Young's moduli, however, were significantly different out of package but converged over time, which may be a function of the load-free implantation for both material types. Mechanical remodeling of both PADM firm and pliable scaffolds is highlighted by an initial loss in ultimate tensile stress. This result is not unexpected given that intact noncross-linked ECM materials have previously been observed to exhibit a similar response.[24] However, this response was concurrent with limited cell infiltration and revascularization (Figure 5). These findings were unexpected, as it had been generally believed that cell infiltration, both fibroblastic and inflammatory, is a mechanism for collagen remodeling and degradation in vivo. In this study, the correlation of minimal–moderate cell infiltration into scaffold materials with maximum remodeling rates does not support this theory. It is possible that proteases and/or other ubiquitous enzymes present in the interstitial spaces surrounding the implant are at least partially responsible for the initial mechanical changes of implanted intact ECM-based scaffolds. A more robust panel of histological stains for specific cell types and collagen quantification along with extended time points may enhance the understanding of PADM remodeling and its role in wound healing within this model.

A second key finding that must be noted is the mechanical recovery capability of implanted PADM scaffolds in vivo. It is imperative to recognize that most biological materials, depending on the production processing, will change once implanted and remodel over time. In vitro collagenase bath digestion assays used to characterize mesh remodeling only provide a catabolic environment for material remodeling;[6] in vivo implantation provides both catabolic and anabolic opportunities. In this study, the minimum ultimate tensile stress of PADM scaffolds did not occur on the final day of evaluation. The minimum lowest ultimate tensile stresses and maximum extension at 30 N of both PADM firm and pliable materials were noted on day 25. Between days 25 and 30, a statistically significant increase in the ultimate tensile stress and a decrease in the extension at 30 N of both PADM materials were observed. The ultimate tensile stress of day 30 samples was not statistically different from day 10 values. A second confirmatory study with PADM firm was executed to verify these results (Tables 2 and 4). The time period of the confirmatory study was extended to 42 days to include two data points beyond the day that the lowest stress levels were noted in the original study. Results from this second study were in agreement with the original study, reproducing and confirming the increase in mechanical properties following approximately 1 month of implantation. This mechanical remodeling of the PADM materials occurred even though scaffolds were not implanted under tension in the subcutaneous pockets. Implanting scaffolds under tension may further increase the ultimate tensile stress of materials, as it is generally accepted that the

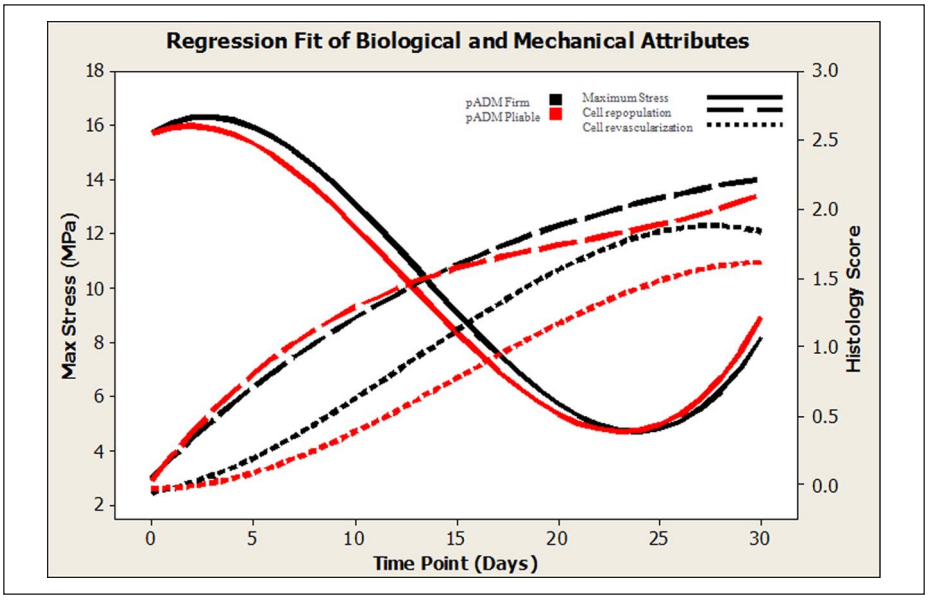

Figure 5. Ultimate tensile stress and histology scores for both PADM firm and pliable materials plotted against time. Cubic regression fit sans error bars were used to plot a summary of the data for clarity. Details for each metric can be found in Tables 1 and 3.
PADM: porcine-derived acellular dermal matrix.

biomechanical remodeling of an implanted material will follow its functional requirement. Therefore, it is presumed that all mechanical remodeling observed in this model was a direct result of the biological response to the implanted material. From the histological analysis, it is evident that the mechanical remodeling noted in these studies was not a function of encapsulation. Encapsulation is characterized by the formation of a capsule around the implant. Neither gross observation nor histology showed any evidence of scarring or significant capsule formation (Figure 4). Although no conclusion can be made with regard to organization of the collagen from the trichrome-stained images alone, this staining does suggest formation of new collagen over time. However, taken together, the trichrome staining and the mechanical evaluation results suggest the formation of new collagen fibers that are organized to provide increased structural integrity of the PADM scaffold over time. The results in this study suggest that the basket-weave organization of the PADM provides a macroporous scaffold for new collagen organization and regeneration. Without the organization of newly formed collagen, a likely disorganized scar tissue with reduced mechanical integrity is likely to form. While the model used in this study offers new methods of relating biological and mechanical changes in implanted materials, it is limited in a number of ways. First, the materials used are not implanted in a clinically relevant setting. The biomechanics experienced in the ventral abdominal wall or breast tissue are substantially different from those in a subcutaneous dorsal pocket on a rat and may result in different responses. To that extent, results obtained in this study are different from the results obtained in a recent study.[25] Briefly, Mulier et al. implanted Strattice in a bridging defect in Sprague-Dawley rats and monitored the biological and mechanical responses of the explants over a period of 1 year. At the 1-month time point, no differences were noted between implanted and control Strattice materials. Furthermore, at the 3-month time point, a steep decrease in the tensile properties of implanted Strattice was noted. In contrast, we observed significant changes at 30 days in implanted scaffold material properties. While our study did not extend to 1 year, a significant increase in the mechanics was noted between days 20 and 30. Additionally, previous primate studies using an interpositional bridge defect[17,26,27] as well as clinical experiences in patients that have been followed for 1 year or more[28] did not demonstrate the extent of remodeling, thinning, or mechanical loss reported in the study by Mulier et al. One explanation for these differences may be that the short-term study presented here (along with the studies in old-world primates[17,26,27] and human experiences) is not representative of a long-term (xenogeneic) response elicited in a rat model. However, one could consider studies in genetically modified small rodents to discern the relative contributions of the immune response.[29] Therefore, repeating these rodent studies for extended periods of time in an athymic animal model may be beneficial.

Another potential limitation with this model is the folds noted in placement of the material. PADM pliable, by design, is produced to be more drapeable than PADM firm and thereby better covers the natural contours of the body. A higher incidence of folds was noted in the PADM pliable material compared with the PADM firm material. This outcome is expected and associated with the challenge of placing a PADM pliable article flat in the subcutaneous tunnel

pocket. Anchoring the sample at the implant corners may be helpful in preventing folds; however, anchoring materials may confound PADM remodeling results. Mechanical attributes of samples wherein a fold occurred in the tested field demonstrated significantly reduced load capacity and failure at the fold site (Table 1). This may indicate a nonuniform susceptibility to endogenous processes. It is hypothesized that folds create pockets in the connective tissue in which interstitial fluids can build and alter the remodeling of the material; alternatively, folds may damage the collagen and make it more susceptible to mechanical failure. A more thorough evaluation of the phenotypic characteristics of the cells infiltrating the ECM scaffold and surrounding space is necessary to fully appreciate the mechanism of biologic matrix reorganization. The work presented here is a first step toward that evaluation.

Conclusions

An understanding of the short-term changes in biological and mechanical attributes of intact ECM scaffolds can be evaluated in a rat subcutaneous model. PADM firm and pliable scaffolds showed similar biological and mechanical remodeling kinetics in this model. Vessel formation and cell infiltration to PADM was evident between 2 and 3 weeks. Mechanical remodeling was highlighted by an initial decrease in ultimate tensile stress not induced by cell infiltration, followed by a significant increase in material strength concurrent with the synthesis and formation of new collagen fibers. Young's moduli of both firm and pliable materials followed similar trends in remodeling. The initial difference noted between the moduli of firm and pliable materials was reduced over time following implantation. Despite the expected initial mechanical decreases, increasing mechanical attributes were noted within the short time period studied and occurred while the implanted matrices maintained a tensile stress capability well in excess of anticipated clinical functional requirements.

Acknowledgements

Editorial assistance was provided by Peloton Advantage, LLC.

Declaration of conflicting interests

The authors are employees of LifeCell Corporation.

Funding

This study was funded by LifeCell Corporation.

References

1. Silverman RP, Li EN, Holton LH, III, et al. Ventral hernia repair using allogenic acellular dermal matrix in a swine model. *Hernia* 2004; 8(4): 336–342.
2. Silverman RP. Acellular dermal matrix in abdominal wall reconstruction. *Aesthet Surg J* 2011; 31(7 Suppl.): 24S–29S.
3. Brewer MB, Rada EM, Milburn ML, et al. Human acellular dermal matrix for ventral hernia repair reduces morbidity in transplant patients. *Hernia* 2011; 15(2): 141–145.
4. Holton LH, Haerian H, Silverman RP, et al. Improving long-term projection in nipple reconstruction using human acellular dermal matrix: an animal model. *Ann Plast Surg* 2005; 55(3): 304–309.
5. Smart NJ, Marshall M and Daniels IR. Biological meshes: a review of their use in abdominal wall hernia repairs. *Surgeon* 2012; 10(3): 159–171.
6. Deeken CR, Eliason BJ, Pichert MD, et al. Differentiation of biologic scaffold materials through physicomechanical, thermal, and enzymatic degradation techniques. *Ann Surg* 2012; 255(3): 595–604.
7. Deeken CR, Faucher KM and Matthews BD. A review of the composition, characteristics, and effectiveness of barrier mesh prostheses utilized for laparoscopic ventral hernia repair. *Surg Endosc* 2012; 26(2): 566–575.
8. Deeken CR, Melman L, Jenkins ED, et al. Histologic and biomechanical evaluation of crosslinked and non-crosslinked biologic meshes in a porcine model of ventral incisional hernia repair. *J Am Coll Surg* 2011; 212(5): 880–888.
9. Barber FA and Aziz-Jacobo J. Biomechanical testing of commercially available soft-tissue augmentation materials. *Arthroscopy* 2009; 25(11): 1233–1239.
10. Yoder JH and Elliott DM. Nonlinear and anisotropic tensile properties of graft materials used in soft tissue applications. *Clin Biomech (Bristol, Avon)* 2010; 25(4): 378–382.
11. Green KA and Lund LR. ECM degrading proteases and tissue remodelling in the mammary gland. *Bioessays* 2005; 27(9): 894–903.
12. Junge K, Binnebosel M, von Trotha KT, et al. Mesh biocompatibility: effects of cellular inflammation and tissue remodelling. *Langenbecks Arch Surg* 2012; 397(2): 255–270.
13. Stamenkovic I. Extracellular matrix remodelling: the role of matrix metalloproteinases. *J Pathol* 2003; 200(4): 448–464.
14. Streuli C. Extracellular matrix remodelling and cellular differentiation. *Curr Opin Cell Biol* 1999; 11(5): 634–640.
15. Badylak SF, Freytes DO and Gilbert TW. Extracellular matrix as a biological scaffold material: structure and function. *Acta Biomater* 2009; 5(1): 1–13.
16. Badylak SF. The extracellular matrix as a scaffold for tissue reconstruction. *Semin Cell Dev Biol* 2002; 13(5): 377–383.
17. Xu H, Wan H, Sandor M, et al. Host response to human acellular dermal matrix transplantation in a primate model of abdominal wall repair. *Tissue Eng Part A* 2008; 14(12): 2009–2019.
18. Connor J, McQuillan D, Sandor M, et al. Retention of structural and biochemical integrity in a biological mesh supports tissue remodeling in a primate abdominal wall model. *Regen Med* 2009; 4(2): 185–195.
19. Abdulla YH, Adams CW and Morgan RS. Connective-tissue reactions to implantation of purified sterol, sterol esters, phosphoglycerides, glycerides and free fatty acids. *J Pathol Bacteriol* 1967; 94(1): 63–71.
20. Bhat KS and Walvekar S. Response of subcutaneous connective tissue to materials and drugs: a simplified technique. *J Endod* 1975; 1(6): 202–204.
21. Grecco AJ, Sakima T, Lia RC, et al. Reaction of the subcutaneous connective tissue of the rat to implants of chemically active acrylic resins. Histologic study. *Ars Curandi Odontol* 1976; 3(2): 15–19.

22. Kidd KR, Nagle RB and Williams SK. Angiogenesis and neovascularization associated with extracellular matrix-modified porous implants. *J Biomed Mater Res* 2002; 59(2): 366–377.
23. Varkey M, Ding J and Tredget EE. Differential collagen-glycosaminoglycan matrix remodeling by superficial and deep dermal fibroblasts: potential therapeutic targets for hypertrophic scar. *Biomaterials* 2011; 32(30): 7581–7591.
24. Weiler A, Hoffmann RF, Bail HJ, et al. Tendon healing in a bone tunnel. Part II: histologic analysis after biodegradable interference fit fixation in a model of anterior cruciate ligament reconstruction in sheep. *Arthroscopy* 2002; 18(2): 124–135.
25. Mulier KE, Nguyen AH, Delaney JP, et al. Comparison of Permacol and Strattice for the repair of abdominal wall defects. *Hernia* 2011; 15(3): 315–319.
26. Chen J, Xu J, Wang A, et al. Scaffolds for tendon and ligament repair: review of the efficacy of commercial products. *Expert Rev Med Devices* 2009; 6(1): 61–73.
27. Sandor M, Xu H, Connor J, et al. Host response to implanted porcine-derived biologic materials in a primate model of abdominal wall repair. *Tissue Eng Part A* 2008; 14(12): 2021–2031.
28. Itani KMF, Rosen M, Vargo D, et al. Prospective study of single-stage repair of contaminated hernias using a biologic porcine tissue matrix: the RICH study. *Surgery* 2012; 152(3): 498–505.
29. Allman AJ, McPherson TB, Badylak SF, et al. Xenogeneic extracellular matrix grafts elicit a TH2-restricted immune response. *Transplantation* 2001; 71(11): 1631–1640.